Available online at www.sciencedirect.com
SCIENCE DIRECT®
Journal of Magnetic Resonance 173 (2005) 90–96
JMR Journal of Magnetic Resonance
www.elsevier.com/locate/jmr

Communication

T_2-shortening of ^{3}He gas by magnetic microspheres

Kevin R. Minard*, Charles Timchalk, Richard A. Corley

Pacific Northwest National Laboratory, P.O. Box 999, Richland, WA 99352, USA

Received 7 October 2004; revised 24 November 2004
Available online 22 December 2004

Abstract

In a gas-filled material like the lung parenchyma, the transverse relaxation time (T_2) for ^{3}He is shortened by the deposition of magnetic microspheres and rapid molecular diffusion through induced field distortions. Here, this unique relaxation process is described theoretically and predicted T_2-shortening is validated using pressurized ^{3}He gas in a foam model of alveolar airways. Results demonstrate that: (1) significant T_2-shortening is induced by microsphere deposition, (2) shortened ^{3}He T_2s are accurately predicted, and (3) measured relaxation times are exploitable for quantifying local deposition patterns. Based on these findings the feasibility of imaging inhaled particulates in vivo with hyperpolarized ^{3}He is examined and performance projections are formulated.

Keywords: T_2; ^{3}He; Gas; Microspheres; MRI

1. Introduction

Magnetic resonance (MR) imaging of hyperpolarized ^{3}He gas is increasingly used for visualizing respiratory structure and function in humans and laboratory animals [1–4]. In these applications the transverse relaxation time (T_2) for inhaled ^{3}He is normally shortened by binary collisions with molecular oxygen [5] and rapid molecular diffusion through susceptibility-induced magnetic field distortions [6]. At 1.5 T, diffusion-mediated susceptibility effects at gas-tissue interfaces dominate and the T_2 for ^{3}He is reduced to ~20 ms in distal airways [6,7], whereas oxygen-limited T_2s of ~10 s are measured at substantially lower static field strengths [8]. In both extremes, T_2 values require careful consideration, especially when interpreting acquired images [6,8] or optimizing T_2-weighted pulmonary imaging protocols [7,8].

Compared with gas relaxation, T_2-shortening in liquids is characterized by different length and time-scales that are dictated by slower molecular mobility. Nevertheless, similar relaxation mechanisms can be important for gas-phase pulmonary imaging. One example already considered in previous work is susceptibility-induced T_2-shortening [6,9]. Another, which is the focus here, is relaxation by molecular diffusion through the local field distortions surrounding a random distribution of impermeable magnetized spheres. In liquids this mechanism is important for understanding shortened T_2s in fat-water emulsions [10], as well as solutions containing paramagnetic ions [11], metalloproteins [12], and superparamagnetic nanoparticles [13]. The same relaxation process has, however, not yet been considered in gases—even though it provides a natural framework not only for assessing the potential utility of gas-phase MR contrast agents but also for visualizing the inhalation of magnetically label materials.

If techniques that exploit the T_2-shortening of hyperpolarized ^{3}He could be developed for detecting magnetic particles in the respiratory tract the underlying approach would likely present new opportunities for visualizing pulmonary drug delivery and assessing the potential hazards associated with inhaled pollutants. However, no general theory for describing T_2-shortening by

* Corresponding author. Fax: +1 509 376 2303.
E-mail address: kevin.minard@pnl.gov (K.R. Minard).

1090-7807/$ - see front matter
doi:10.1016/j.jmr.2004.11.026

magnetized spheres in distal airways has yet been developed to provide the foundation for such a capability. Fortunately, recent formulations of outer sphere (OS) relaxation theory are applicable under conditions that are well satisfied when magnetic microspheres are dispersed as an aerosol in ^{3}He gas. Here, the formal aspects of OS theory are briefly reviewed and arguments are presented for extending its applicability to describe diffusion-dominated surface relaxation when ^{3}He permeates a porous material like the lung and magnetic microspheres are dispersed over its surfaces. Mathematical expressions for predicting enhanced gas relaxation are then validated using pressurized ^{3}He in a foam model of alveolar airways and the feasibility of imaging the deposition of inhaled particles in the respiratory tract with hyperpolarized ^{3}He is examined.

2. Theoretical considerations

Recent work summarizes the formal aspects of OS theory and its use for describing the relaxation of solvent molecules as they diffuse in a dilute solution of impermeable spheres with uniform size and magnetic properties [13,14]. Generally, this is applicable if temporary binding does not occur at sphere surfaces and relaxation is considered in the motional averaging limit [10–14]. Under these conditions microscopic distortions in the local magnetic field are described by the root mean square angular frequency shift ($\Delta\omega_r$) for a spin at the surface of an isolated sphere, and a single timescale (τ_D) characterizes diffusion-mediated spin de-phasing. By convention, τ_D is defined in terms of the sphere radius (r) and the diffusion coefficient (D) for detected spins, such that [13,14]:

$$\tau_D = r^2/D, \tag{1}$$

and magnetostatics shows [15]:

$$\Delta\omega_r = \sqrt{\frac{4}{5}}\gamma B_{eq} = \sqrt{\frac{4}{5}}\gamma\mu/r^3 = (8\pi/3)\gamma M/\sqrt{5}, \tag{2}$$

γ being their gyromagnetic ratio, B_{eq} the equatorial magnetic field for an isolated sphere, μ is its magnetic moment, and M its magnetization (CGS units assumed throughout).

Under the conditions already specified OS theory can be rigorously applied to derive analytical expressions that describe the reduced T_1 and T_2 values for ^{3}He gas in an aerosol containing dispersed magnetic microspheres. In a high static magnetic field (B_0) when the magnetic energy for each sphere (μB_0) is much greater than its thermal energy, and the Larmor precession frequency (ω_0) is much greater than $1/\tau_D$, little T_1-shortening is expected and the OS contribution to the enhanced T_2 relaxation rate is proportional to the volume fraction (v) of dispersed microspheres in gas-filled spaces, such that [16,17]:

$$[1/T_2]_{OS} = (4/9)v\tau_D(\Delta\omega_r)^2. \tag{3}$$

Except for the leading numerical constant (4/9), this enhancement is identical to that derived for *permeable* spheres using alternative formulations [18,19]. In that case, however, a leading constant of 2/5 is found and this small difference has been attributed to the assumption of unrestricted diffusion [20], whereas explicit boundary conditions excluding diffusing spins from inside spheres are specified within the OS framework.

In a Carr–Purcell–Meiboom–Gill (CPMG) experiment, which is commonly used measuring T_2 relaxation times, the amount of spin de-phasing during the refocusing time between successive 180° RF pulses ($\tau_{refocus}$) is expected to be large for strongly magnetized spheres. In this case, $\Delta\omega_r\ \tau_{refocus} \gg 1$, and Monte Carlo simulations demonstrate that the motional averaging condition can be safely assumed, provided [16]:

$$\Delta\omega_r\tau_D < 3. \tag{4}$$

Less certain is how gas relaxation might be affected after an aerosol is introduced into a porous material like the lung where microspheres can then settle on a large surface area. To examine this issue it is helpful to first consider the well-known Brownstein–Tarr model of surface relaxation in a spherical pore of radius a [21]. In this case, the total transverse magnetization for a gas within the pore is expected to decay with a single exponential at a diffusion-limited rate that is enhanced by $(1/T_2)_s \times (3s/a)$ [22]. Generally, this is valid provided that [22]:

$$(sa/2D) \times (1/T_2)_s \ll 1, \tag{5}$$

where s denotes the thickness of the surface layer containing magnetic microspheres, and $(1/T_2)_s$ represents the enhanced transverse relaxation rate for gas within it.

When Eq. (5) is satisfied the Brownstein–Tarr model predicts an enhanced T_2 relaxation rate that is identical to Eq. (3). To illustrate this, first consider the case when magnetic spheres are deposited only on the pore surface and assume that within the surface layer ^{3}He relaxation is governed by Eq. (3). Then, $(1/T_2)_s$ in the Brownstein–Tarr model is given by 4/9 $v'\tau_D\ (\Delta\omega_r)^2$, where v' is now the volume fraction of magnetic spheres within the surface layer. Thus, the relaxation enhancement predicted for diffusion-dominated surface relaxation is (4/9) $v'\tau_D\ (\Delta\omega_r)^2 \times (3s/a)$. However, if the spherical pore is initially filled with an aerosol containing magnetic microspheres with a volume fraction v—then v' is just $va/3s$ and Eq. (3) is again obtained. Consequently, OS theory and the Brownstein–Tarr model give comparable results. Therefore, details regarding the precise pattern of pore-scale microsphere deposition appear unimportant since OS theory is strictly derived for a random distribution of spheres whereas the Brownstein–Tarr formulation describes relaxation when spheres are deposited only on pore surfaces.

3. Materials and methods

Considerations outlined in the previous section indicate that OS theory can be employed for predicting the T_2-shortening of ^{3}He gas by magnetic microspheres—even if the gas permeates a porous material like the lung and microspheres are dispersed over its internal surfaces. To test this hypothesis, ^{3}He MR measurements were performed at 2.0 T using a foam model of alveolar airways. The model is depicted in Fig. 1A and consists of four removable foam cylinders that are each loaded with a different volume fraction (v) of magnetic microspheres. Each cylinder has a diameter of 1 centimeter (cm) and a length of 5 cm. The foam itself also has an open, interconnected air space, and optical images presented in Fig. 1B show that its voids are comparable to the size of alveolar ducts in lung tissue.

Magnetic microspheres with a mean radius (r) of 1 μm were purchased (product # 70-00-203, Micromod, Germany) for validation studies since particles of this size are known to penetrate deep into the lung when inhaled [23]. The microspheres are comprised of magnetite (Fe_3O_4, 40% w/w) in a poly(lactic acid) (PLA) matrix and are green fluorescent. Optical microscopy provided by the manufacturer indicates that individual microsphere size is highly uniform and measurements of microsphere motion in a magnetic field gradient of known strength indicates that microsphere magnetization (M) saturates above 1 T at ~21.1 emu/cm^3 [24]. Given that the gyromagnetic ratio (γ) for ^{3}He is $20381(\mathrm{G\,s})^{-1}$, Eq. (2) then indicates that the RMS frequency shift $\Delta\omega_r$ is about $1.61\times10^6\ (\mathrm{s})^{-1}$ for validation measurements performed at 2.0 T.

During shipment from the manufacturer magnetic microspheres are stored as an aqueous suspension containing 1.7×10^8 per ml. Upon receipt, microspheres were re-suspended using 20 W of high-intensity ultrasound and, immediately after, five different solutions were prepared in which the volume fraction of microspheres was 0, 10^{-4}, 10^{-5}, 10^{-6}, and 10^{-7}. In all solutions, microspheres were suspended at a pH of 7.8 based on manufacturer recommendation. This was achieved using a volatile buffer that consisted of titrated HCl in a 0.1 M solution of triethanolamine. To deposit a known volume fraction (v) of magnetic microspheres in the gas-filled spaces of each foam cylinder—foam was first immersed in one of the prepared particle suspensions. After trapped air was removed under vacuum the fluid saturated foam was then frozen. Frozen liquid was then removed via sublimation using a standard lyophilizer. After drying, cylindrical foam samples were then placed in the sample holder shown in Fig. 1A.

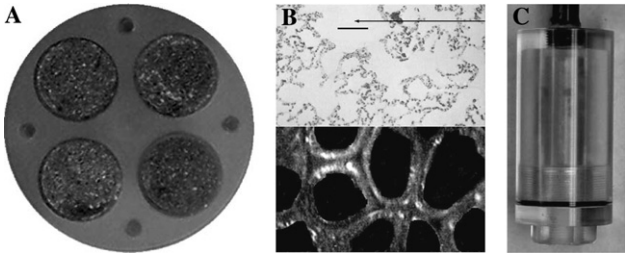

Fig. 1. Materials. (A) Lung model consisting of four removable foam cylinders that are loaded with different volume fractions (v) of magnetic microspheres. (B) Top: Light microscopy of excised lung tissue (bar is 100 μm long); Bottom: Light microscopy of foam showing a field-of-view with the same size. The pore structure of the foam is comparable to the size of alveolar ducts (top arrow). (C) MR compatible pressure vessel. Prior to MR experiments gas is introduced through a 1/4 in. PVC pipe that is seen at the top of the vessel. Opposite the PVC inlet, the chamber seals with a large threaded cap and a rubber O-ring. When the cap is unscrewed the interior of the chamber is accessible—so foam samples can be introduced or removed. The pressure vessel, threaded cap, and sample holder (shown in A) are all machined from acrylic.

Since the manufacturer recommended 320 W of ultrasonic power to ensure minimal particle agglomeration upon re-suspension, and a device capable of generating this was not available, the possibility of particle agglomeration was examined. To determine the size of particles dispersed in foam samples microsphere suspensions identical to those already described were analyzed using a commercial system that determines particle size distributions based on the principle of light extinction (Accusizer C770, Particle Sizing Systems, Santa Barbara, CA). Results indicated that particle agglomeration was indeed significant since measured particle radii were all above the 1-micron-radius of individual microspheres (data not shown). Results also indicated that the effective radius of agglomerated particles was Gaussian distributed with a mean and standard deviation of 4.6 and 2.7 μm, respectively. In light of this finding, a value of 4.6×10^{-4} cm was used for the sphere radius (r) that appears in Eq. (3) through Eq. (1). It is also noted that particle agglomeration has no other effect on either $\Delta\omega_r$ or v since Eq. (2) is independent of the sphere radius and the volume fraction filled by many individual microspheres or fewer agglomerates is the same.

Prior to ^{3}He MR studies foam samples were placed inside the custom fabricated pressure vessel depicted in Fig. 1C. The vessel was then pressurized to 150 psi using a mixture of N_2, ^{3}He, and O_2. During this process N_2 and ^{3}He was supplied at 140 psi using a lecture bottle that contained 2% N_2 and 98% ^{3}He (Spectra Gas, Branchburg, NJ). The final pressure was then achieved by adding ~10 psi of O_2 in order to shorten the T_1 for ^{3}He inside [5]. Afterward, magnetic resonance was performed using a Varian Unity Plus console (Palo Alto, CA) and a 30-cm-diameter, horizontal-bore, magnet (Oxford, UK) equipped with a homebuilt birdcage coil and commercial gradients (RRI, Billerica, MA).

Once the pressure vessel was placed inside the MR magnet a transverse 2D ^{3}He image of permeating gas

was acquired and regions-of-interests (ROIs) were planned for localized measurements of ^{3}He gas relaxation in each foam cylinder. In order to maximize the signal-to-noise ratio (SNR) for quantitative relaxation measurements ROI dimensions were chosen to encompass each foam cylinder in its entirety. The MR signal originating from permeating gas was then localized using STEAM [25] and, as previously described [26,27], magnetization preparation with either inversion recovery or a CPMG pulse sequence was exploited for localized T_1 and T_2 measurements. In these experiments the echo-time (TE) within the STEAM portion of the pulse sequence was fixed at 2.5 ms and a 9 s repetition time (TR) was employed to minimize saturation effects. The diffusion coefficient for ^{3}He gas diffusion was also measured using a STEAM sequence but this had a longer TE (4 ms) in order to accommodate additional pulsed field gradients for sensitizing the MR response to molecular diffusion. Standard analysis of diffusion-weighted STEAM data yielded a ^{3}He diffusion coefficient (D) of 0.13 ± 0.01 cm^2/s. The diffusion time-scale (τ_D) was therefore 1.63 μs and the product $\Delta\omega_r\tau_D$ was ~2.6, thereby, satisfying Eq. (4) and suggesting that OS theory could be employed for comparing CPMG data with theoretical expectations.

In all CPMG experiments a refocusing time ($\tau_{refocus}$) of 250 μs was employed. After localization with STEAM, T_2-weighted ^{3}He NMR spectra were generated via the Fourier transformation of raw time-domain data. T_2 values were then obtained by nonlinear least squares fitting to the peak heights measured for different CPMG echo-times. The same CPMG preparation used for STEAM experiments was then used in conjunction with 2D Constant Time Imaging [27,28]—and the same nonlinear least squares fitting was employed on a pixel-by-pixel basis for generating a T_2 map from the magnitude of different T_2-weighted images. Here, constant time imaging (CTI) was employed because diffusion induced blurring and signal loss are both minimized with this pure phase-encoding method [29], and in this context, CTI and similar methods are well-suited for gas-phase MR applications [30]. For the current study, 2D, T_2-weighted, CTI data were collected using a hard, nonselective RF excitation and magnetization in the transverse plane was imaged using 32 phase-encoding steps along each orthogonal axis. To minimize diffusion losses the (encoding) time between the excitation pulse and the end of applied phase-encoding gradients was only 180 μs and the SNR was further enhanced using two signal averages. For each phase encoding step a single complex pair was acquired using a 400 Hz bandwidth and after all phase encoding was completed standard 2D Fourier reconstruction was applied. With a TR of 1.5 s between successive encoding steps—each 2D, T_2-weighted, constant-time image required ~50 min to collect.

To exploit estimated T_2 values for determining the volume fraction (v) of magnetic microspheres deposited in gas-filled spaces it is first emphasized that Eq. (3) only describes the effect of magnetic particulates on gas relaxation and *does not* account for relaxation by paramagnetic oxygen [5] or magnetic susceptibility variations at gas-foam interfaces [6]. Both of these loss mechanisms are, however, additive. Therefore, the effects of magnetic particulates are isolated if the T_2-relaxation rate for ^{3}He gas in a representative (control) region containing no particles ($[1/T_2]_{control}$) is subtracted from that measured in a region with particles ($[1/T_2]_{particles}$). The local volume fraction for magnetic particulates in the latter is then calculated using Eq. (3), such that:

$$v = \left\{ \left[\frac{1}{T_2}\right]_{particles} - \left[\frac{1}{T_2}\right]_{control} \right\} (9/4) \Big/ \left(\tau_D \Delta\omega_r^2\right). \qquad (6)$$

4. Results

Fig. 2A shows a transverse MR image of pressurized ^{3}He gas in a foam model of alveolar airspaces and the white box depicts a typical region-of-interest (ROI) for localized CPMG-STEAM measurements. Importantly, the ROI shown could be centered on different cylinders to interrogate local gas properties and examine the effect of magnetic microsphere deposition. Fig. 2B shows how the MR signal for ^{3}He gas in different cylinders varies with echo-time (TE) in localized CPMG-STEAM experiments. In the plot dots represent experimental data acquired using different cylinders and the solid lines represent nonlinear least squares fitting to an

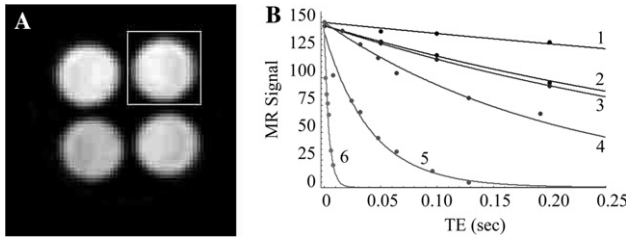

Fig. 2. T_2-shortening measured using localized CPMG-STEAM. (A) 2D CTI of pressurized ^{3}He gas. The white box depicts a typical region-of-interest used for performing localized T_2 measurements with CPMG-STEAM. (B) CPMG data showing the localized MR signal strength (shaded dots) for pressurized ^{3}He gas in different cylinders as a function of increasing echo-time (TE). In all cases data was acquired using at least seven different echo-times but all data is not visible in the limited range shown. Solid lines represent numerical nonlinear least squire fits to a single exponential decay—and derived relaxation times are summarized in Table 1. Curve 1 is for an empty cylinder containing no foam or microspheres, curve 2 is for foam containing no microspheres, curve 3 if for foam prepared with a volume fraction (v) of magnetic microspheres equal to 10^{-7}, curve 4 is for foam with $v = 10^{-6}$, curve 5 is for foam with $v = 10^{-5}$, and curve 6 is for foam with $v = 10^{-4}$.

exponential decay measured with at least seven different echo-times. In all experiments 32 averages were employed and, with a 9.0 s TR, data for each cylinder typically required ~1/2 h to collect.

Curve 1 in Fig. 2B shows the relaxation decay for pressurized ^{3}He gas in an empty cylinder that contains no foam or particles. The curve is seen to exhibit the slowest signal decay and the measured T_2 is close to the 1.8 s measured for T_1. The next fastest transverse signal decay is exhibited by curve 2—which depicts the signal for ^{3}He gas in foam without particles. The difference between curves 1 and 2 is therefore entirely due to the presence of the foam and presumably a result of variations in magnetic susceptibility at gas/foam interfaces [6]. Curve 3 represents the next fastest decay and is for ^{3}He in foam containing magnetic microspheres dispersed with a volume fraction of only 10^{-7}. Even at this low concentration a discernable difference with the signal decay in curve 2 is evident, and curves 4–6 show that successively faster signal loss is observed in foam samples prepared with higher particle concentrations. Table 1 summarizes the T_2 values derived from each curve together with the prepared volume fraction of magnetic microspheres (v). The T_2 for ^{3}He gas in foam samples is seen to decrease with increasing v and calculated volume fractions for magnetic microspheres based on Eq. (6) agree well with prepared values over 3 orders of magnitude.

To demonstrate how the above analysis can be combined with gas-phase MR imaging CTI experiments were performed with variable T_2-weighting. Figs. 3A–E each show a 2D, T_2-weighted, constant time image of four different foam cylinders. Each image is from a series of 16 that all depict the same samples but are characterized by different CPMG echo-times. Each foam cylinder was prepared with a different volume fraction of magnetic microspheres and each T_2-weighted, ^{3}He image is normalized by the brightest pixel to illustrate how differences in microsphere concentration alter observed CTI contrast with increasing CPMG echo-time (TE). To increase the SNR for imaging more oxygen was employed so the T_1 for ^{3}He gas was shortened to about 0.4 s. Since each 2D, T_2-weighted, constant time image required ~50 min to collect—the entire series of 16 required ~13.5 h to acquire. The colorized image in Fig. 3F summarizes imaging results and represents a T_2-map that is derived by analyzing the MR signal decay on a pixel-by-pixel basis. The calibrated color scale to the right relates T_2 values to the local volume fraction of magnetic microspheres and exploits Eq. (6) together with the mean relaxation rate measured for foam containing no particles. Generally, calculated volume fractions based on measured T_2's agree within ~15% of the prepared values given in the figure caption. Results in Fig. 3 therefore not only validate theoretical predictions based on Eq. (3) but also demonstrate that CTI can be successfully employed for quantifying heterogeneous microsphere deposition in a porous material with a microstructure like the lung's.

5. Discussion

In this study, outer sphere (OS) relaxation theory was employed for describing the T_2-shortening of ^{3}He gas in an aerosol containing strongly magnetized microspheres, and arguments were presented for extending its applicability to describe diffusion-dominated surface relaxation when ^{3}He permeates a porous material like the lung and magnetic microspheres are dispersed over pore surfaces. Analytical expressions for predicting enhanced gas relaxation were then validated using pressurized ^{3}He in a foam model of alveolar airways. Results therefore provide a quantitative basis for examining the feasibility of exploiting hyperpolarized (HP) ^{3}He for imaging the deposition of magnetic particulates in the distal airways of the lung.

Upon inhalation, ^{3}He gas is close to atmospheric pressure so its diffusion rate is significantly higher than in the current study. In the distal airways, however, mixture with air serves to decrease ^{3}He mobility since it must then diffuse among heavier gas molecules. As a result, the diffusion coefficient for a binary ^{3}He–gas mixture is significantly less than for pure ^{3}He and has

Table 1
Data summary for localized CPMG-STEAM measurements

Curve #	Prepared particle density (v)	Measured T_2 for ^{3}He gas (ms)	Calculated particle density (v)
1	−0	1500 ± 50	Not applicable
2	+0	480 ± 13	Control in Eq. (6)
3	10^{-7}	433 ± 6	$(1.2 \pm 0.1) \times 10^{-7}$
4	10^{-6}	220 ± 13	$(1.3 \pm 0.1) \times 10^{-6}$
5	10^{-5}	41 ± 4	$(1.2 \pm 0.1) \times 10^{-5}$
6	10^{-4}	4.0 ± 0.5	$(1.3 \pm 0.2) \times 10^{-4}$

Each curve in Fig. 2B shows how the MR signal for ^{3}He gas in a different cylinder varies with increasing echo-time (TE) in a localized CPMG-STEAM experiment. The Table summarizes—(1) the prepared particle density for each cylinder, (2) the measured T_2 for ^{3}He gas, and (3) the calculated particle density based on Eq. (6). Errors on all T_2 values represent the uncertainty in nonlinear least squares estimates and their propagation via Eq. (6) determines the uncertainty in calculated values for the volume fraction (v) of magnetic microspheres. For cylinders without particles: (−) indicates that data was acquired without foam and (+) indicates the presence of foam.

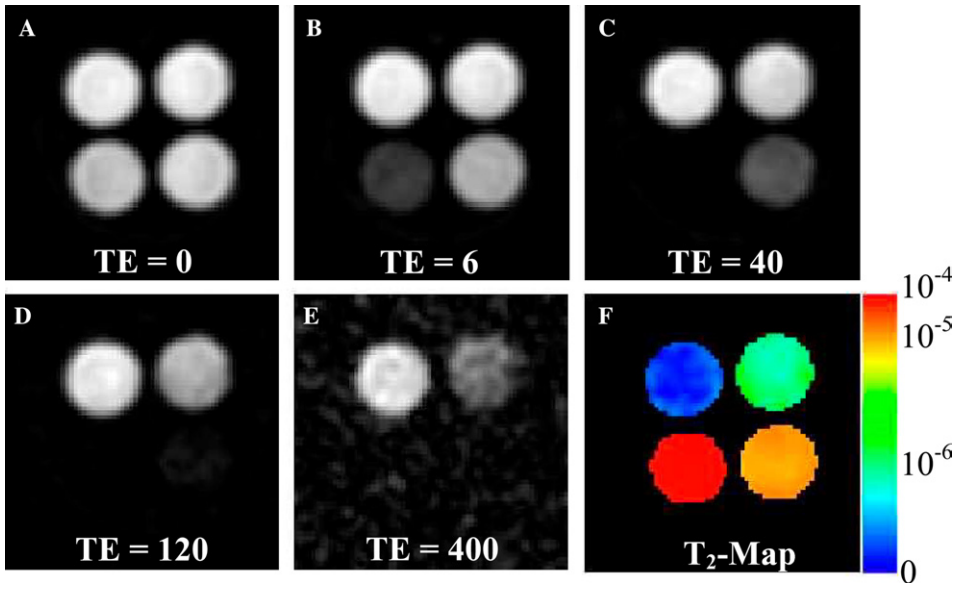

Fig. 3. Quantitative microsphere imaging with ^{3}He CTI. (A–E) T_2-weighted MR images acquired with different CPMG echo-times (TE's given in milliseconds). The images are from a series of more than 16 that all depict the same foam samples. The field of view in each image is 4 cm on a side and planar resolution is 1.25 mm. (F) Colorized T_2 map derived using a pixel-by-pixel analysis of all gas-phase MR image data. The calibrated scale allows T_2 values in each pixel to be translated into a local volume fraction for deposited magnetic microspheres using Eq. (6) and the average T_2 measured in foam without magnetic microspheres. The foam cylinder on the upper left has no microspheres, and moving clockwise, the prepared volume fraction (v) in each foam cylinder is 10^{-6}, 10^{-5}, and 10^{-4}. Average T_2 values derived from image analysis are 232 ± 8, 156 ± 10, 39 ± 3, and 4.4 ± 0.4 ms, respectively.

been estimated to be 0.86 cm^2/s in distal airways [31]. Given that this more closely characterizes the speed with which ^{3}He moves among deposited microspheres this diffusion coefficient is employed here for formulating OS predictions under in vivo conditions.

One consequence of ^{3}He's greater mobility in vivo is that susceptibility induced phase accumulation is motionally averaged and can no longer be refocused with applied RF so T_2^* is equal to T_2 [6]. At 1.5 T the T_2^* for ^{3}He gas in the deep lung has been measured to be ~20 ms [6,7]. This is therefore significantly shorter than the T_2 measured here for ^{3}He in foam containing no magnetic microspheres. Nevertheless, assuming in vivo experiments are performed at 1.5 T using the same microspheres, that their magnetization remains saturated, and aggregated particles with the same size (i.e., $r = 4.6$ μm) are deposited—$\Delta\omega_r\,\tau_D$ equals 0.4 and theoretical expressions validated in this study are applicable.

In the current study a 10% change in T_2 was the minimum necessary to confidently detect the presence of magnetic microspheres and quantify their local volume fraction using Eq. (6). Assuming the same requirement for in vivo imaging applications then means that a minimum volume fraction of $\sim 2 \times 10^{-5}$ might be detectable in a single resolved volume element within a ^{3}He image. Given that the increased sensitivity afforded with a hyperpolarized gas has been exploited for resolving voxels with a volume of as little as 6.4×10^{-6} cm^3 in the lung of a live rat [32], a volume fraction of 2×10^{-5} represents less than 1 magnetic particle per resolved volume element. In vivo projections based on validation experiments presented here therefore suggest that it may be feasible to exploit T_2-weighted ^{3}He imaging for detecting the presence of single magnetic particle in the lung of a live rat.

Of course, there are potential difficulties with exploiting the T_2-shortening of ^{3}He gas for visualizing microsphere deposition in vivo. For example, quantification of local volume fractions based on Eq. (6) would require the registration of two separate T_2 maps—one acquired before inhalation and one after. Consequently, registration errors could degrade results—especially since the T_2 for ^{3}He appears quite heterogeneous [6]. Moreover, in vivo imaging times and required gas consumption are potentially problematic. If, for example, two T_2 maps were created and each utilized 3D images acquired using five different echo-times, then the protocols previously used for visualizing rat airways with voxel volumes of 6.4×10^{-6} cm^3 would require ~16 L of hyperpolarized ^{3}He and raw T_2-weighted image data would require ~3.5 h to collect [32]. Of course, imaging could always be done on two separate occasions—but even in this case the timely production of required gas necessitates substantial improvements in existing technology for HP gas generation. In light of these considerations 2D studies like those previous used for measuring the ^{3}He T_2 in the guinea pig lung [6] may initially be more feasible for quantitative particle dosimetry in vivo. Even under those circumstances, however, technical difficulties might still arise because ^{3}He is largely insoluble in water. Consequently, it remains unclear whether microsphere

impaction in the lung's mucus layer may cause errors in measured deposition patterns. Nevertheless, the prospects of single particle detection are tantalizing and, if related logistical and technological challenges can be surmounted, such a capability could have far reaching implications to inhalation toxicology, pulmonary drug delivery, and other related research.

Acknowledgments

Research was performed in the Environmental Molecular Sciences Laboratory (a national scientific user facility sponsored by the US Department of Energy's Office of Biological and Environmental Research) located at Pacific Northwest National Laboratory (PNNL), and operated for DOE by Battelle. Financial support was provided by NIH NHLBI RO1 HL073598, and Project Nos. 46109 and 40403 of PNNL's Laboratory Directed Research and Development (LDRD) program.

References

[1] H.U. Kauczor, Hyperpolarized helium-3 gas magnetic resonance imaging of the lung, Top. Magn. Reson. Imaging 14 (2003) 223–230.
[2] B.T. Chen, A.C.S. Brau, A.G. Johnson, Measurement of regional lung function in rats using hyperpolarized ^{3}Helium dynamic MRI, Magn. Reson. Med. 49 (2003) 78–88.
[3] D.A. Yablonskiy, A.L. Sukstanskii, J.C. Leawoods, D.S. Gierada, G.L. Bretthorst, S.S. Lefrak, J.D. Cooper, M.S. Conradi, Quantitative in vivo assessment of lung microstructure at the alveolar level with hyperpolarized 3He diffusion MRI, Proc. Natl. Acad. Sci. USA 99 (2002) 3111–3116.
[4] M. Viallon, G.P. Cofer, S.A. Suddarth, H.E. Moller, X.J. Chen, M.S. Chawla, L.W. Hedlund, Y. Cremillieux, G.A. Johnson, Functional MR microscopy of the lung using hyperpolarized ^{3}He, Magn. Reson. Med. 41 (1999) 787–792.
[5] B. Saam, W. Happer, H. Middleton, Nuclear relaxation of ^{3}He in the presence of O_2, Phys. Rev. A 52 (1) (1995) 862–865.
[6] X.J. Chen, H.E. Moller, M.S. Chawla, G.P. Cofer, B. Driehuys, L.W. Hedlund, J.R. MacFall, G.A. Johnson, Spatially resolved measurements of hyperpolarized gas properties in the lung in vivo. part II: T_2^*, Magn. Reson. Med. 42 (1999) 729–737.
[7] B. Saam, D.A. Yablonskiy, D.S. Gierada, M.S. Conradi, Rapid imaging of hyperpolarized gas using EPI, Magn. Reson. Med. 42 (1999) 507–514.
[8] E. Durand, G. Guillot, L. Darrasse, G. Tastevin, P.J. Nacher, A. Vignaud, D. Vattolo, J. Bittoun, CPMG measurements and ultrafast imaging in human lungs with hyperpolarized Helium-3 at low field (0.1 T), Magn. Reson. Med. 47 (2002) 75–81.
[9] J.H. Jensen, R. Chandra, Strong field behavior of the NMR signal from magnetically heterogeneous tissues, Magn. Reson. Med. 43 (2000) 226–236.
[10] L. Marciani, C. Ramanathan, D.J. Tyler, P. Young, P. Manoj, M. Wickham, A. Fillery-Travis, R.C. Spiller, P.A. Gowland, Fat emulsification measured using NMR transverse relaxation, J. Magn. Reson. 153 (2001) 1–6.
[11] P. Gillis, S.H. Koenig, Transverse relaxation of solvent protons induced by magnetized spheres: application to ferritin, erythrocytes, and magnetite, Magn. Reson. Med. 5 (1987) 323–345.
[12] Y. Gossuin, A. Roch, R.N. Muller, P. Gillis, Relaxation induced by ferritin and ferritin-like magnetic particles: the role of proton exchange, Magn. Reson. Med. 43 (2000) 237–243.
[13] S.H. Koenig, K.E. Kellar, Theory of $1/T_1$ and $1/T_2$ NMRD profiles of solutions of magnetic nanoparticles, Magn. Reson. Med. 34 (1995) 227–233.
[14] P. Gillis, A. Roch, R.A. Brooks, Corrected equations for susceptibility-induced T_2-shortening, J. Magn. Reson. 137 (1999) 402–407.
[15] J.D. Jackson, Classical Electrodynamics, 2nd ed., Wiley, New York, 1975.
[16] P. Gillis, F. Moiny, R.A. Brooks, On T_2-shortening by strongly magnetized spheres: a partial refocusing model, Magn. Reson. Med. 47 (2002) 257–263.
[17] R.A. Brooks, F. Moiny, P. Gillis, On T_2-Shortening by weakly magnetized particles: the chemical exchange model, Magn. Reson. Med. 45 (2001) 1014–1020.
[18] J.H. Jensen, R. Chandra, NMR relaxation in tissues with weak magnetic field inhomogeneities, Magn. Reson. Med. 44 (2000) 144–156.
[19] A.L. Sukstanskii, D.A. Yablonskiy, Gaussian approximation in the theory of MR signal formation in the presence of structure-specific magnetic field inhomogeneities, J. Magn. Reson. 163 (2003) 236–247.
[20] Y. Gossuin, P. Gillis, F. Lo Bue, Susceptibility-induced T_2-shortening and unrestricted diffusion, Magn. Reson. Med. 47 (2002) 194–195.
[21] K.R. Brownstein, C.E. Tarr, Importance of classical diffusion in NMR studies of water in biological cells, Phys. Rev. A 19 (1979) 2446–2453.
[22] S. Godefroy, J.P. Korb, M. Fleury, R.G. Bryant, Surface nuclear magnetic relaxation and dynamics of water and oil in macroporous media, Phys. Rev. E 64 (2001) 021605.
[23] H.C. Yeh, R.F. Phalen, O.G. Raabe, Factors influencing the deposition of inhaled particles, Environ. Health Perspect. 15 (1976) 147–156.
[24] U.O. Hafeli, R. Ciocan, J.P. Dailey, Characterization of magnetic particles and microspheres and their magnetophoretic mobility using a digital microscopy method, Eur. Cells Mater. 3 (2) (2002) 24–27.
[25] J. Frahm, K.-D. Merboldt, W. Hanicke, Localized proton spectroscopy using stimulated echoes, J. Magn. Reson. 72 (1987) 502–508.
[26] K.R. Minard, X. Guo, R.A. Wind, Quantitative ^{1}H MRI and MRS microscopy of individual V79 lung tumor spheroids, J. Magn. Reson. 133 (1998) 368–373.
[27] S.D. Beyea, B.J. Balcom, P.J. Prado, A.R. Cross, C.B. Kennedy, R.L. Armstrong, T.W. Bremner, Relaxation time mapping of short T_2^* nuceli with single-point imaging (SPI) methods, J. Magn. Reson. 135 (1998) 156–164.
[28] S. Gravina, D.G. Cory, Sensitivity and resolution of constant-time imaging, J. Magn. Reson. 104 (Series B) (1994) 53–61.
[29] S. Choi, X.-W. Tang, D.G. Cory, Constant time imaging approaches to NMR microscopy, Int. J. Imaging Systems Techn. 8 (1997) 263–276.
[30] P.J. Prado, B.J. Balcom, I.V. Mastikhin, A.R. Cross, R.L. Armstrong, A. Logan, Magnetic resonance imaging of gases: a single-point ramped imaging with T_1 enhancement (SPRITE) study, J. Magn. Reson. 137 (1999) 324–332.
[31] X.J. Chen, H.E. Moller, M.S. Chawla, G.P. Cofer, B. Driehuys, L.W. Hedlund, G.A. Johnson, Spatially resolved measurements of hyperpolarized gas properties in the lung in vivo. Part I: diffusion coefficient, Magn. Reson. Med. 42 (1999) 721–728.
[32] G.A. Johnson, G.P. Cofer, L.W. Hedlund, R.R. Maronpot, S.A. Suddarth, Registered ^{1}H and ^{3}He magnetic resonance microscopy of the lung, Magn. Reson. Med. 45 (2001) 365–370.